Clean Techn Environ Policy (2016) 18:949–956
DOI 10.1007/s10098-015-1040-8

ORIGINAL PAPER

Development and materials characteristics of fly ash- slag-based grout for use in sulfate-rich environments

Yang Yuyou[1] · Cui Zengdi[2] · Li Xiangqian[1] · Dou Haijun[1]

Received: 30 June 2015 / Accepted: 14 September 2015 / Published online: 18 September 2015

Abstract This study improves cement–water glass two-shot grouting materials by adding fly ash and slag, making a new kind of anti-seepage grouting material for the prevention of soil contamination. The chemical corrosion mechanism and chemical resistance properties of the new grouting material were studied, and the contamination prevention performance of the anti-seepage system in complex geological environments, such as tailings ponds and heavy metal-contaminated sites, was also evaluated. The basic properties of the grouting materials, including stability and mobility, were tested. Sodium sulfate was used to corrode the grout gels after demolding, and the effects of chemical corrosion on mechanical properties were tested by unconfined compressive strength tests. The strength of the solution gels increased rather than decreased when fly ash and slag were added. The effect of chemical corrosion on grouting material composition was analyzed by X-ray diffraction. The results show that $CaSO_4 \cdot 2H_2O$ crystals have a higher diffraction peak under sodium sulfate corrosion than in standard curing conditions. This difference explains the reason for the increasing strength of the material. The effect of chemical corrosion on the gels' microstructure was analyzed by SEM. Numbers of clubbed tri-sulfur calcium sulphoaluminate and diamond-shaped gypsum crystals were found.

✉ Yang Yuyou
yangyuyou@cugb.edu.cn

[1] School of Engineering and Technology, China University of Geosciences (Beijing), Beijing 100083, China

[2] School of Engineering and Computer Science, University of the Pacific, Stockton 95211, USA

Keywords Soil pollutants · Chemical corrosion · Grouting material · Strength

Introduction

Considerable amounts of solid waste are generated during the extraction, beneficiation, and processing of minerals. Generally speaking, production of 1 ton of copper generates 110 tons of waste ore and 200 tons of overburden (Earthworks and Oxfam America 2004). Mine drainage contains various heavy metals such as Cu, Zn, As, and Pb (Singovszka et al. 2015). These heavy metals also exist in mine solid waste.

The mining waste is usually stored in tailings pond, which inevitably contributes to the environmental deterioration with acid mine drainage, heavy metal migration, and groundwater contamination, for tens of years. In order to control the soil contamination induced by tailings pond full of pollutants, grouting treatment is commonly applied to the ponds along with some other control measures. Grouting is one effective method for controlling soil contamination.

Grouting as an anti-seepage technology is widely used in tailing ponds to prevent heavy metal migration and impede the expansion of contaminated areas. However, pollutants generated from mining wastes could change the soil pH and chemical composition. The strength loss rate of blocks is about 30 % in acid environment (Yang et al. 2013). In these conditions, traditional cement grout is susceptible to corrosion and has poor cementation functions (Chen et al. 2011). Thus, it is important to improve the corrosion resistance of grouting material to reduce contamination of the surrounding soil and water.

Some scholars have studied the strength loss and chemical corrosion problems of cement grouting system under polluted geological environments. Ghafoori et al. (2015) found that replacing a portion of cement with fly ash was useful in reducing expansion of the studied concretes exposed to sulfate. Xing et al. (2009) found that Cl^- makes a difference to the early, mid-, and long-term strength of cement-soil, and SO_4^{2-} mainly impacts the long-term strength of cement-soil. Han et al. (2014) researched the corrosion mechanism of cement-soil induced by $MgCl_2$ and established the regression equation between corrosion strength and normal strength of the block. Ye et al. (2014) studied the corrosion mechanism of cement induced by sulfate and found that sulfate content increased by 92 % in the surface of slag cement blocks after sulfate corrosion, the ratio of Portland cement is 115.2 %, and the compressive strength is far higher than that of Portland cement. Yao et al. (2014) improved anti-corrosion performance of marine concrete utilizing coal combustion byproducts and blast furnace slag. These studies enriched the theory of grouting material corrosion induced by groundwater pollution. But developing grouting material with resistance to chemical attack is still the key to solve the problem of soil pollutants' seepage control.

Flowability and stability of grout have indirect effects on the control of soil pollutants. Low flowability and stability will increase the difficulty of injection and result in bad impermeability of anti-seepage system. In this study, bentonite and naphthalene water reducer are used to adjust the new grouting materials.

Based on the heretofore problems, this study improved cement–water glass two-shot grout and investigated its corrosion resistance properties. The major issues include stability and flowability of grout and corrosion strength of improved grout gels. X-ray diffraction and scanning electron microscopy were also used to analyze the composition and microstructure of grout. This new grouting material reutilizes industrial wastes fly ash and slag on the one hand and treats heavy metal contamination on the other hand, thus it has sound economic and social benefits.

Materials and methods

Raw materials

The new grouting material was designed on the basis of traditional cement–water glass two-shot grouting. The alkali-activated effect of sodium silicate on fly ash and slag was also considered. At room temperature, water glass activates slag slowly (Altan and Erdogan 2012). The alkaline activation of fly ash used with water glass solution produces an alkaline aluminosilicate (Mužek et al. 2012). The main ingredients include cement, slag, fly ash, and water glass. Some additives such as sodium bentonite and naphthalene water reducer (β-naphthalenesulfonic acid formaldehyde condensate) are used to improve the performance of the grout. The slag (SL) in this experiment was produced by Capital Jade (Beijing) Business Co., Ltd, with a specific surface area of 448 m^2/kg. Fly ash (FA) is a class-II ash (Chinese standard GB 1596-2005), produced by Tianjin Huapanshan Power Plant Co., Ltd., with a specific surface area of 516 m^2/kg. Water glass was produced by Beijing Hongxing Guangsha Chemical Construction Materials Co., Ltd., with a modulus of 2.6 and a Baume degree of 45°Bé. The major composition of water glass is sodium silicate. The cement, produced by Hebei Yutian Chuncheng Cement Co., Ltd., is 42.5 grade ordinary Portland cement and has a specific surface area of 370 m^2/kg. The chemical composition and grain size distribution of cement, fly ash, and slag were also tested. The results are shown in Tables 1 and 2.

Specimen preparation

First, the composite grout is prepared, then its stability and flowability are tested to evaluate its working performance. Cement, fly ash, slag, and water are mixed together to make grout A. There are three types of grout A, one made from pure cement, one from cement and fly ash, and the other from cement, fly ash, and slag. The ratio of each raw material of grout A is shown in detail in Table 3. Then, Baume degree of water glass is adjusted to 35°Bé as grout B. The Baume degree of water glass was diluted from 45°Bé to 35°Bé by water. It was tested by a Baume hydrometer while diluting. Lastly, grouts A and B are mixed at the volume ratio of 1:0.2 (A:B) to make grout C. The compositions of grout C are shown in Table 3. Table 4 shows the chemical composition and physical properties of grout B.

Grout C is poured into molds sized 70.7 mm × 70.7 mm × 70.7 mm and into demolds 24 h later. Test blocks are prepared in two groups and in triplicate. Group 1 is cured in standard conditions (20 ± 2 °C, humidity: 95 %) for 90 days. Group 2 is cured in sodium sulfate solution, other conditions being the same as in Group 1. The mass concentration of sodium sulfate is 5 %.

Stability and flowability test methods

The stability of grouting materials is expressed as bleeding ratio. After being kept static for a period of time, the grout will show solid–liquid separation due to the sedimentation of solid particles. The ratio of supernatant liquid is defined as bleeding ratio. In the test, 200 ml grout was taken in a graduated cylinder and placed on a level surface. The

Table 1 Chemical composition of raw materials

Raw materials	Mass fraction (%)							
	SiO_2	Al_2O_3	Fe_2O_3	CaO	MgO	SO_3	Loss	f-CaO
Slag	33.84	11.68	2.2	38.13	10.61	1.98	2.56	0.05
Fly ash	57.62	28.59	4.21	3.46	0.64	0.40	5.78	0.35
Cement	22.61	4.35	2.46	62.60	1.91	2.89	1.74	0.71

Table 2 Grain size distribution of cement, fly ash, and slag

Grain size (μm)	<2.40	2.40–4.97	4.97–10.28	10.28–21.28	21.28–34.56	34.56–44.04	44.04–56.13	>56.13
Slag	15.69	13.89	22.92	33.07	13.08	1.26	0.09	0
Fly ash	21.74	19.09	15.95	17.24	11.68	5.12	4.18	5.00
Cement	11.51	9.95	17.63	30.85	19.37	5.95	3.19	1.55

Table 3 Raw material ratios of grouts A and C

Number	Components of grout A						Volume ratio of A:B
	Cement (%)	Fly ash (%)	Slag (%)	Sodium bentonite (%)	Naphthalene water reducer (%)	Water–cement ratio	
A1	100	–	–	0, 0.5, 1.0, 2, 3	–	0.8	–
A2	40	60	–	0, 0.5, 1.0, 2, 3	–	0.8	–
A3	40	45	15	0, 0.5, 1.0, 2, 3	–	0.8	–
A4	100	–	–	–	0, 0.2, 0.5, 1.0, 1.5	0.8	–
A5	40	60	–	–	0, 0.2, 0.5, 1.0, 1.5	0.8	–
A6	40	45	15	–	0, 0.2, 0.5, 1.0, 1.5	0.8	–
C1	100	–	–	3	1.5	0.8	1:0.2
C2	40	60	–	3	1.5	0.8	1:0.2
C3	40	45	15	3	1.5	0.8	1:0.2

Table 4 Chemical composition/physical properties of grout B

Chemical composition	Sodium silicate and water
Modulus (SiO_2/Na_2O)	2.6
Baume degree (°Bé)	35
Density (g/cm^3)	1.32

volume of the supernatant liquid was recorded every 20 min until three continuous records were the same. The flowability is expressed as viscosity. The viscosity of the grout was tested by a six-speed rotational viscometer.

Chemical corrosion test method

The unconfined compressive strength of standard test blocks (cured in standard conditions) and chemically corroded blocks was tested after they reached their designed curing age. The strength of the blocks was tested on a strength testing machine (CSS WAW 2000DL) designed by Changchun Testing Machine Institute. The chemical resistance of gels was studied by comparing the strength of corroded blocks with that of standard ones. The strength loss rate (η) is expressed as Eq. (1):

$$\eta = \frac{q_{us} - q_{uc}}{q_{us}} \times 100\,\%, \tag{1}$$

where q_{us}(MPa) denotes the unconfined compressive strength of test blocks under standard curing condition and q_{uc}(MPa) denotes that of test blocks under corrosion condition. The following mentioned standard strength corresponds to q_{us} while corrosion strength to q_{uc}.

Composition and microstructure tests

When the designed curing age was reached, the blocks of grout C were crushed into powder and sieved through a 200-mesh screen and dried under vacuum, after which X-ray diffraction tests were conducted through a D/MAX-RBX-ray diffractometer produced by Rigaku Corporation. The microstructure of gels was examined by a JEM-6301F field emission scanning electron microscope.

Results and discussion

Stability test results of grout A

Bleeding ratios of grout A with different sodium bentonite contents were tested and presented in Fig. 1. The figure shows that blocks in the three cases all have a relatively high bleeding ratio if bentonite was not added. Bleeding ratio of cement grout (A1) was the largest, exceeding 25 %. When slag or fly ash (A2, A3) was added, the bleeding ratios were lower than those of cement grout (A1) all the time. This may be a result of the high content of fine particles in slag and fly ash. The bleeding ratios dropped sharply with the increase of bentonite content, but did slow when the bentonite content exceeded 1 %. Sodium bentonite can decrease free water content by water absorption and forming network, thereby decreasing the bleeding ratio. Bleeding ratios of the three kinds of grout A were approximately equal when bentonite content reached 3 %. According to the Technical Specification for Cement Grouting Construction of Hydraulic Structures (DL/T 5148-2012), the bleeding ratio of stable grout should not exceed 5 %. Some studies found that the increase of bentonite content will weaken the strength of the blocks (Jiang et al. 2012). With 3 % bentonite, all the grouts had a bleeding ratio of less than 5 %, and therefore it is the optimum bentonite ratio in this test.

Flowability test results of grout A

Flowability is expressed as viscosity. The lower the viscosity is, the bigger the diffusion radius of a grout is and the smaller the grouting pressure is needed. On the contrary, the higher the viscosity is, the more difficult it is for a grout to be injected into a stratum. Therefore, good flowability is very important to ensure effective anti-seepage grouting for soil pollutants. Naphthalene water reducer was used to adjust the viscosity of the grouts. Variation of viscosity with naphthalene water reducer is shown in Fig. 2.

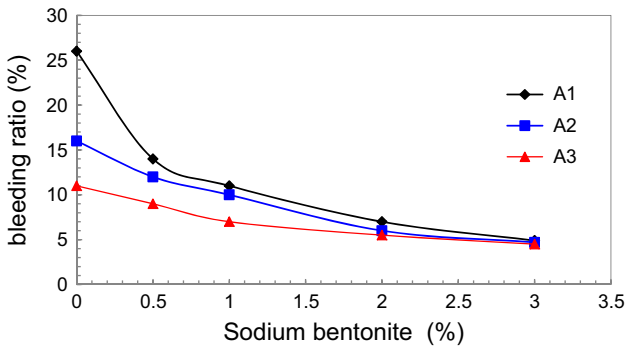

Fig. 1 Variation of bleeding ratio with sodium bentonite

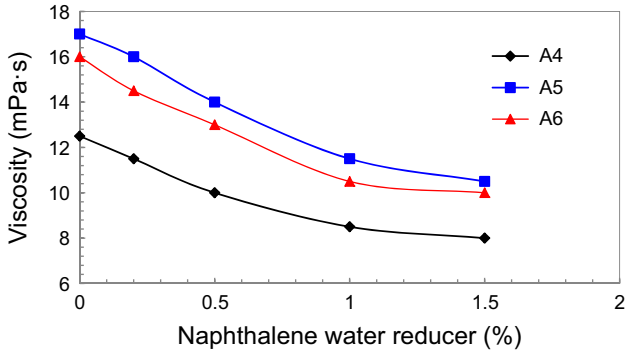

Fig. 2 Variation of viscosity with naphthalene water reducer

As shown in Fig. 2, viscosity decreases with increasing water reducer content. Viscosity decreases rapidly when the content of water reducer is below 1 %, but it does more slowly if higher than 1 %. Therefore, 1 % can be regarded as a reasonable ratio of water reducer. The figure also shows that adding fly ash would increase the grout viscosity, but the effect would be weakened if some fly ash were replaced by slag.

Sulfate corrosion test results

Sulfate corrosion of cement gel is an ubiquitous phenomenon. Gypsum production by sulfate and $Ca(OH)_2$ is the main reason of corrosion (Al-Amoudi 1998). In this study, blocks of C1, C2, and C3 were corroded by sodium sulfate solution for 90 days. Unconfined compressive strength was tested after corrosion. Average strength of the three specimens is calculated. The limits of error are marked for each sample in figures. Results of the sulfate corrosion test are shown in Fig. 3. As shown in Fig. 3a, the corrosion strength of C2 and C3 is higher than their standard curing strength. Strength of C2 in both cases is the lowest. Some research shows that compressive strength will decrease when the ratio of fly ash added to cement exceeds 10 % (Wang 2014). The strength development at early ages is affected negatively with the addition of fly ash in cement (Kocak and Nas 2014). The ratio of fly ash in C2 is 60 % which is the main cause of strength decrease. Strength of C3 in both cases is the highest, because slag reduces the negative influences of fly ash and improves the particle size distribution. In addition, slag is easier to be affected by sodium silicate than fly ash. The mechanism of sulfate corrosion is that $Ca(OH)_2$ and calcium sulphoaluminate react with SO_4^{2-}, producing gypsum and ettringite. The reaction equations involved are shown as follows (Al-Amoudi 1998):

$$Ca(OH)_2 + Na_2SO_4 + 2H_2O \rightarrow CaSO_4 \cdot 2H_2O + 2NaOH \quad (2)$$

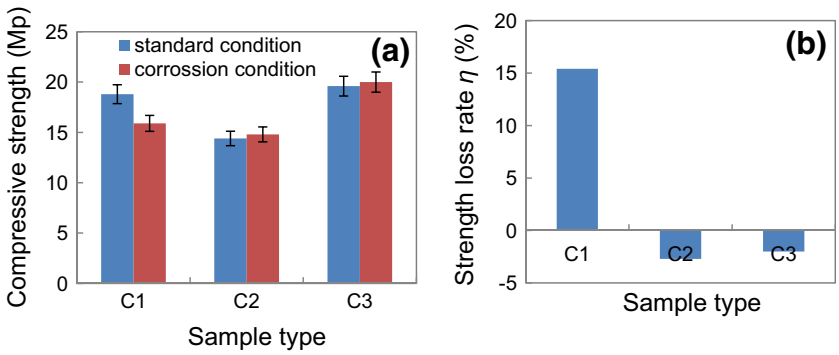

Fig. 3 Variation of compressive strength and strength loss rate in sulfate: **a** compressive strength and **b** strength loss rate in sodium carbonate solution

$$3CaO \cdot Al_2O_3 \cdot CaSO_4 \cdot 18H_2O + 2(CaSO_4 \cdot 2H_2O) + 10H_2O \rightarrow 3CaO \cdot Al_2O_3 \cdot 3CaSO_4 \cdot 32H_2O \quad (3)$$

$$3CaO \cdot Al_2O_3 + 3(CaSO_4 \cdot 2H_2O) + 26H_2O \rightarrow 3CaO \cdot Al_2O_3 \cdot 3CaSO_4 \cdot 32H_2O. \quad (4)$$

There is abundant $Ca(OH)_2$ in C1, favorable for reaction (2). The gypsum and calcium sulphoaluminate crystals continually developing lead to tension in the pores, destruction of structure, and strength decrease. As shown in Table 1, the ratio of CaO in cement is 62.6 % which is much higher than those in fly ash and slag. In C2 and C3, however, lower cement content results in lower $Ca(OH)_2$ and calcium sulphoaluminate contents, so reactions (2), (3), and (4) are hindered. The reaction products can fill the pores without damaging the structure. That is why the corrosion strengths of C2 and C3 are higher than their standard strengths. Figure 3b shows that the strength loss rates of C2 and C3 are much lower than that of C1. This demonstrates that fly ash and slag can improve sulfate corrosion resistance of cement grouting material.

X-ray diffraction and microstructure analysis

X-ray diffraction analysis

The samples of C1, C2, and C3 cured in standard and sulfate conditions were tested by X-ray diffractometer. The diffraction patterns are shown in Fig. 4. When the patterns of sulfate-corroded samples of C1, C2, and C3 (Fig. 4a, b, c) are compared, it can be seen that the peak (29.5°, 2θ) of $CaCO_3$ in C2 and C3 is enhanced. The peak (29.5°, 2θ) of C3 is the highest, even higher than the standard (Fig. 4c). This proves that a considerable amount of $CaCO_3$ is produced in C3 in sulfate environment.

In Fig. 4a, the $Ca(OH)_2$ peak of sulfate-corroded C1 sample decreases compared with the standard case, the peak of $CaSO_2 \cdot 2H_2O$ (31°, 2θ) rises, and a peak of Aft (9°, 16°, 2θ) occurs. This demonstrates that Na_2SO_4 has reacted

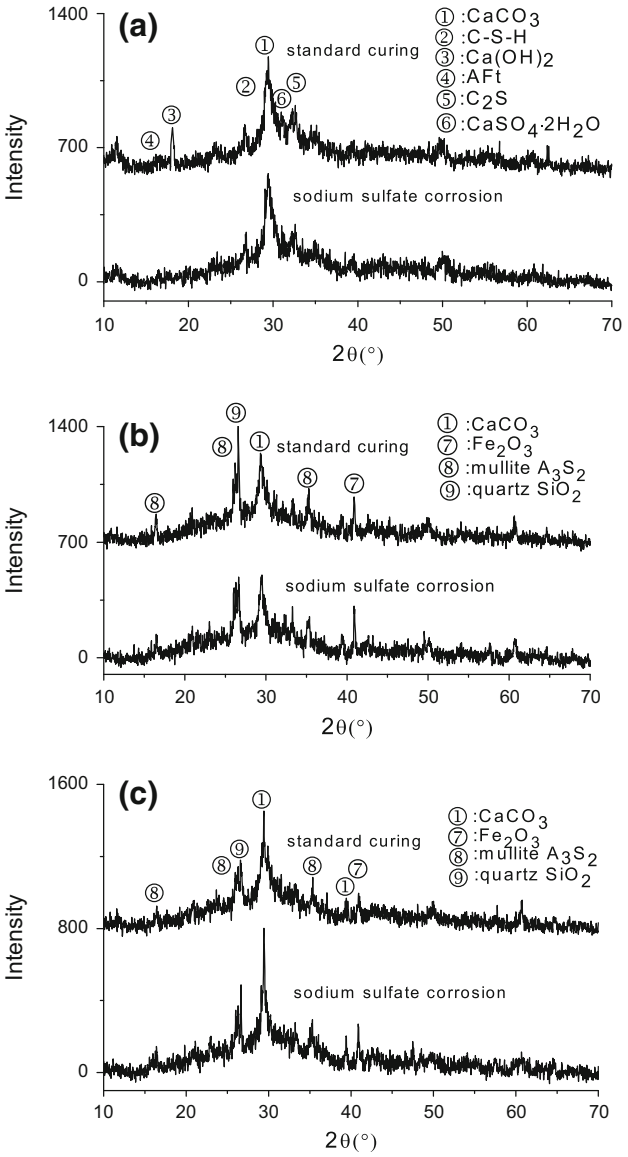

Fig. 4 XRD patterns of specimens: **a** C1 XRD patterns, **b** C2 XRD patterns, and **c** C3 XRD patterns

with $Ca(OH)_2$ and produced gypsum and ettringite. $Ca(OH)_2$ and SiO_2 can have pozzolanic reactions (Hanehara et al. 2001). This indicates that pozzolanic reaction is

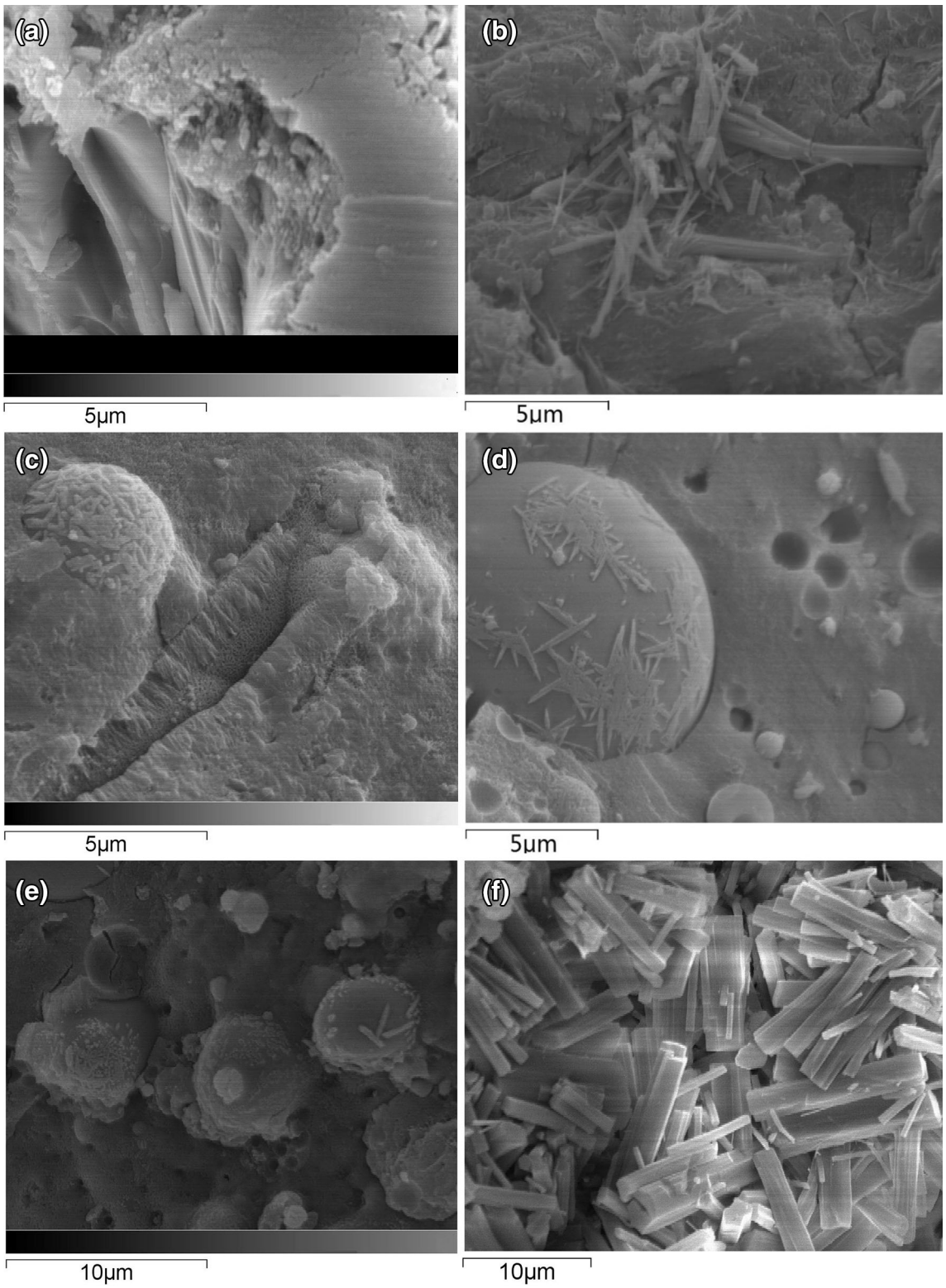

Fig. 5 SEM images of specimens cured for 90 days under standard conditions: **a** C1, **c** C2, and **e** C3. SEM images of specimens cured for 90 days under sodium sulfate: **b** C1, **d** C2, and **f** C3

hindered. The peak of $CaSO_2{\cdot}2H_2O$ is not found in the corrosion patterns of C2 and C3. So there was not much $CaSO_2{\cdot}2H_2O$ produced. In the patterns of C2 and C3, the peak of Fe_2O_3 (40.9°, 2θ) is obvious. And the peak in corrosion patterns is higher than that in standard patterns. $Ca(OH)_2$ can be consumed by Na_2SO_4 in the corrosion

sample of C2 and C3. The lack of $Ca(OH)_2$ may suppress the hydration reaction of C4AF which contains Fe_2O_3. The peak of mullite A_3S_2 at 35.3° is also found in the patterns of C2 and C3. In the standard patterns of C2 (Fig. 4b), the quartz peak at 36.5° (2θ) is relatively high. It is one of the reasons for the low standard strength of C2.

Scanning electron microscope analysis

At the curing age of 90 days, $Ca(OH)_2$ and C–S–H become compact and some fibroid C–S–H fills the pores in C1 (Fig. 5a). More hydration products appear around the fly ash particles (Fig. 5c). This shows that pozzolanic activation has been fully underway. There are also large quantities of amorphous gels, which may be zeolite with geopolymer characteristic.

After 90 days of sulfate corrosion, the structure of C1 is looser than the standard case, and there are large numbers of clubbed tri-sulfur calcium sulphoaluminate and diamond-shaped gypsum crystals (Fig. 5b). The expansibility of gypsum and ettringite lowers the strength of C1. There are some clubbed ettringite and hexagonal columnar single-sulfur calcium sulphoaluminate filling the pores in C2 and C3 (Fig. 5d, f). The reaction of SO_4^{2-} and hydrated calcium aluminate produces ettringite, and then tri-sulfur calcium sulphoaluminate reacts with ettringite, producing single-sulfur calcium sulphoaluminate. The cement contents in C2 and C3 are lower than in C1, so the ettringite and calcium sulphoaluminate produced are only enough to fill the pores. This is a main reason for the strength increase of C2 and C3 in sulfate condition. In Fig. 5c and e, many micropores are found, which may be related to fly ash and slag. Micropores can make structure loose while, on the other hand, providing growth space for ettringite and gypsum. This contributes to avoid structure damage by expansibility. In Fig. 5d, some acicular hydration products are found on the surface of waste residue particles. In Fig. 5c and e, the hydration products are flocculent and surround the waste residue particles. Pozzolanic reaction product of fly ash fills the already-formed pore structure, thus helping to achieve a more compact pore structure and higher strength (Zeng et al. 2012). In the SEM images of corroded C3, some prismatic ettringite is found.

Conclusions

Laboratory tests were carried out to investigate the basic properties of a new grouting material for soil pollutant controlling. Based on the test results, the following conclusions can be obtained:

(1) Bentonite can improve the stability of paste. With 3 % bentonite, the three kinds of grout have a bleeding ratio of less than 5 %. Naphthalene water reducer can reduce the grout viscosity. If naphthalene water reducer content exceeds 1 %, water reducer cannot further reduce grout viscosity.

(2) The strength loss rates of C2 and C3 both are much lower than that of C1. But grout C2 is not suitable for controlling soil pollutants due to its lower strength. The strengths of C2 in standard and corrosion conditions are 14.4 and 14.8 MPa, both are lower than that of C1 in corrosion conditions.

(3) Sulfate corrodes gels because the gypsum and ettringite produced cause tension in the pores and destroy the structure. Adding fly ash and slag can significantly improve the sulfate corrosion resistance of gels. When fly ash and slag are added, the strength under sulfate corrosion is even higher than that in standard curing condition.

In conclusion, this new anti-seepage grouting material has better sulfate corrosion resistance. Much industrial waste residue is reutilized. Much cement is saved. So, the grouting material contains low carbon and contributes to environmental protection. As a matter of policy, mining companies should consider applying anti-seepage grouting material for all ponds used for storing any mining solid waste, collecting all leachate produced, and treating it before discharging into the environment. Effectiveness of the anti-seepage grouting material should be tested by monitoring ground water contamination in the vicinity of the disposal sites.

Acknowledgments The research work described herein was funded by the National Nature Science Foundation of China (NSFC) (Grant Nos. 41472278, 41202220), the Fundamental Research Funds for the Central Universities, China (Grant No. 2652015066), and the Beijing Nova Program (No. 2015B071). These financial supports are gratefully acknowledged.

References

Al-Amoudi OSB (1998) Sulfate attack and reinforcement corrosion in plain and blended cements exposed to sulfate environments. Build Environ 33(1):53–61. doi:10.1016/S0360-1323(97)00022-X

Altan E, Erdoğan ST (2012) Alkali activation of a slag at ambient and elevated temperatures. Cem Concr Compos 34(2):131–139. doi:10.1016/j.cemconcomp.2011.08.003

Chen L, Du Y, Liu S, Jin F (2011) Experimental study of stress-strain properties of cement treated lead-contaminated soils. Rock Soil Mech 32(3):715–721. doi:10.3969/j.issn.1000-7598.2011.03.013

Earthworks, Oxfam America (2004) Dirty metal: mining communities and environment. Earthworks, Washington D.C

Ghafoori N, Najimi M, Diawara H, Islam MS (2015) Effects of class F fly ash on sulfate resistance of Type V Portland cement concretes under continuous and interrupted sulfate exposures.

Constr Build Mater 78:85–91. doi:10.1016/j.conbuildmat.2015.01.004

Han P, Zhang W, Bai X, Tong T (2014) Corrosion mechanism of cemented soil in $MgCl_2$ solution. Kem Ind 63(9–10):311–316. doi:10.15255/KUI.2013.025

Hanehara S, Tomosawa F, Kobayakawa M, Hwang KR (2001) Effects of water/powder ratio, mixing ratio of fly ash, and curing temperature on pozzolanic reaction of fly ash in cement paste. Cem Concr Res 31(1):31–39. doi:10.1016/S0008-8846(00)00441-5

Jiang L, Wang T, Ding G, Chu H, Hu J, Na B, Xiong C (2012) Researches on performances and mechanism of bentonite-cement mortar. New Build Mater 4:48–53. doi:10.3969/j.issn.1001-702X.2012.04.015 **(in Chinese)**

Kocak Y, Nas S (2014) The effect of using fly ash on the strength and hydration characteristics of blended cements. Constr Build Mater 73:25–32. doi:10.1016/j.conbuildmat.2014.09.048

Mužek MN, Zelić J, Jozić D (2012) Microstructural characteristics of geopolymers based on alkali-activated fly ash. Chem Biochem Eng Q 26(2):89–95

Singovszka E, Balintova M, Holub M (2015) Heavy metal contamination and its indexing approach for sediment in Smolnik creek (Slovakia). Clean Technol Environ Policy. doi:10.1007/s10098-015-0991-0

Wang XY (2014) Effect of fly ash on properties evolution of cement based materials. Constr Build Mater 69:32–40. doi:10.1016/j.conbuildmat.2014.07.029

Xing H, Yang X, Xu C, Ye G (2009) Strength characteristics and mechanisms of salt-rich soil–cement. Eng Geol 103(1):33–38. doi:10.1016/j.enggeo.2008.07.011

Yang Y, Wang G, Xie S, Tu X, Huang X (2013) Effect of mechanical property of cemented soil under the different pH value. Appl Clay Sci 79(7):19–24. doi:10.1016/j.clay.2013.02.014

Yao Y, Gong JK, Cui Z (2014) Anti-corrosion performance and microstructure analysis on a marine concrete utilizing coal combustion byproducts and blast furnace slag. Clean Technol Environ Policy 16(3):545–554. doi:10.1007/s10098-013-0654-y

Ye Q, Shen C, Sun S, Chen R, Song H (2014) The sulfate corrosion resistance behavior of slag cement mortar. Constr Build Mater 71:202–209. doi:10.1016/j.conbuildmat.2014.08.019

Zeng Q, Li K, Fen-chong T, Dangla P (2012) Determination of cement hydration and pozzolanic reaction extents for fly-ash cement pastes. Constr Build Mater 27(1):560–569. doi:10.1016/j.conbuildmat.2011.07.007